An investigation of pressure-induced loss of electronic interlayer state and of metallization in ionic solid Li_3N

A. Lazicki[1,2,5], C. S. Yoo[3], W. J. Evans[1], M. Y. Hu[4], P. Chow[4], and W. E. Pickett[2]
[1] *Lawrence Livermore National Laboratory, Livermore, California 94550*
[2] *Physics Department, University of California, Davis, California 95616*
[3] *Washington State University, Pullman, Washington 99164*
[4] *HPCAT/APS, Argonne National Laboratory, Argonne, Illinois 60439 and*
[5] *Current Address: Geophysical Laboratory, Carnegie Institution of Washington, Washington, D. C. 20015*

X-ray diffraction and nitrogen k-edge X-Ray Raman Scattering (XRS) investigations of the crystal and electronic structure of ionic compound Li_3N across two high pressure phase transitions are conducted in a diamond anvil cell and results interpreted using density functional theory. A low-energy peak in the XRS spectrum which is observed in both low-pressure hexagonal phases of Li_3N and absent in the high pressure cubic phase is found to originate from an interlayer band similar to the important free-electronlike state present in the graphite and graphite intercalated systems. XRS detection of the interlayer state is made possible because of its strong hybridization with the nitrogen p-bands. A pressure-induced increase in the band gap of the high pressure cubic phase of Li_3N is shown to originate from the differing pressure dependencies of different quantum-number bands and is revealed as a general feature in low-Z closed-shell ionic materials.

INTRODUCTION

Lithium nitride is the only known thermodynamically stable alkali metal nitride and is one of the most ionic of all known nitrides. At ambient pressure, the nitrogen exists in an anomalous multiply charged (N^{3-}) state [1, 2] which is stable only because of its crystal environment - a hexagonal bipyramid of Li^+ ions [3, 4]. This material is a superionic conductor via vacancy-induced Li^+ diffusion within the Li_2N layers [5–7]. Its potential for use as an electrolyte in lithium batteries [4], a hydrogen storage medium [8–11] and a component in the synthesis of GaN [12] have prompted several studies including investigations into its behavior at high pressure [13, 14].

It has been demonstrated that Li_3N retains its ionic character up to very high pressure, while undergoing a significant structural transition [14]. Inelastic x-ray scattering experiments as well as first-principles calculations reveal that this structural change is accompanied by distinct changes in the electronic bands. Electronic changes accompanying pressure-driven structural phase transitions in covalently bonded materials (such as graphite and boron nitride) are relatively well understood because their directional bonding is affected in a predictable way by changes in the local crystal environment. However, in non-directionally-bonded closed-shell ionic materials the situation is more subtle and electronic changes not as well documented. Here we explore the origins of these changes and identify an important feature in the bandstructure; an interlayer band (to the best of our knowledge, observed here for the first time in an ionic solid) which was previously understood to have Li 2s character [1].

Additionally, a pressure-driven widening of the electronic band gap is examined and related to an expected rapid increase in energy of the conduction bands relative to the valence bands, as a result of their higher principle quantum number and kinetic energy. Neighboring compounds Li_2O and LiF are shown to exhibit similar band-gap increases demonstrating that this appears to be the norm for second-row closed-shell ionic solids.

EXPERIMENTAL DETAILS

Polycrystalline lithium nitride powder (99.5 % purity, CERAC, Inc) was loaded into a membrane diamond-anvil cell of designed at Lawrence Livermore National Laboratory. Several diamond sizes were used to obtain an extended range of pressure up to 200 GPa. In the lower pressure experiments, argon was used as a pressure medium and internal pressure standard. For the high-pressure experiments, no pressure medium was used, and copper or ruby chips (Al_2O_3:Cr^{3+}) were included in the sample chamber as pressure indicators. Under non-hydrostatic conditions, we found that the equation of state fitting parameters differed moderately from those obtained under quasi-hydrostatic conditions; by 8.7%, 0.8% and 13.2% for the zero pressure bulk modulus (B_o), unit cell volume (V_o) and pressure derivative of bulk modulus (B_o'), respectively. Samples were loaded in an argon environment to protect hygroscopic Li_3N from reaction with moisture in the air. High-pressure behavior was investigated by angle-dispersive powder x-ray diffraction (ADXD) and inelastic x-ray Raman scattering (XRS) at high pressure beamlines 16IDB and 16IDD, respectively, at the Advanced Photon Source (APS) at Argonne National Laboratory. For the ADXD experiments, we used intense monochromatic x-rays (λ = 0.3683 or 0.4126 Å) microfocused to $\sim$10 μm at the sample using a pair of piezo-crystal controlled bimorphic mirrors. X-ray diffraction patterns were recorded on a high-resolution image plate detector (MAR 350) and analyzed with the

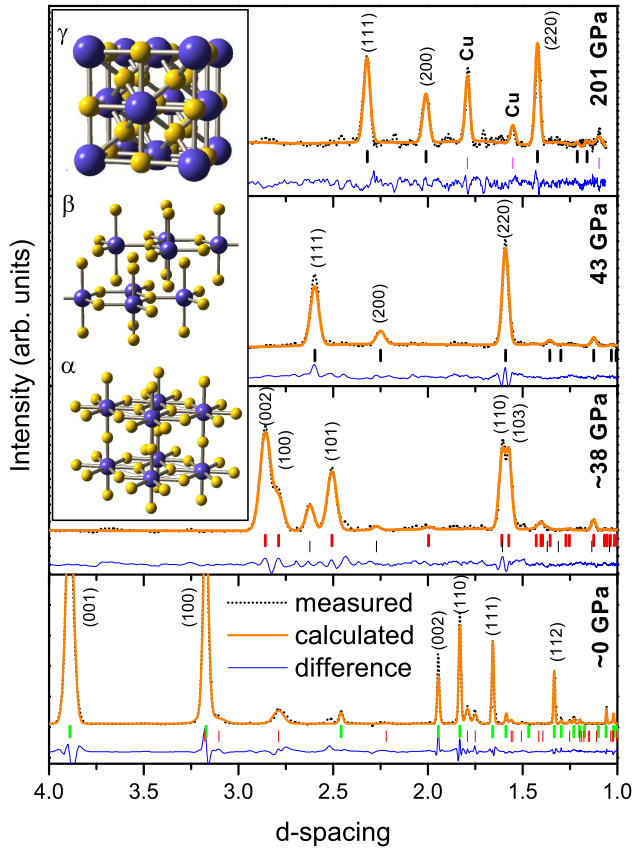

FIG. 1: (Color online) ADXD patterns of Li_3N at ambient pressure (a mixture of α and β hexagonal phases), at ~38 GPa (β phase, directly prior to the phase transition), at 43 GPa (γ phase, directly following the phase transition), and at 201 GPa (γ phase, with additional reflections from copper pressure indicator). Refined and difference patterns from the GSAS Rietveld refinement are shown. (hkl) reflections from each phase are shown in green (α), red (β), black (γ), and magenta (copper). The crystal structures of each phase are shown, with larger spheres representing the nitrogen ions, smaller representing lithium.

FIT2D [15], XRDA [16] and GSAS (EXPGUI) [17] programs. For the XRS experiments, we used monochromatic x-rays (9.687 keV or 0.0128 Å) focused to ~20 x 50 μm at the sample through an x-ray translucent Be gasket by a pair of 1 m-long Kirkpatrick-Baez focusing mirrors. Six spherically bent Si(660) single crystal analyzers (50 mm in diameter) were vertically mounted on a 870 mm Rowland circle to refocus inelastically scattered x-ray photons onto a Si detector (Amp Tek) at a scattering angle of 25° in a nearly back scattering geometry (Bragg angle of 88.6°). This configuration corresponds to a momentum transfer of q ~2.2 $Å^{-1}$. The overall system provides an energy resolution of ~1 eV.

COMPUTATIONAL DETAILS

First-principles electronic structure calculations were performed to explore and clarify the electronic changes occurring under pressure. Because of the large six-fold compression carried out in these calculations, we used two methods for comparison: full-potential linearized augmented plane-waves (LAPW) as implemented in WIEN2k code [18] within the Generalized Gradient Approximation [20] and a full-potential nonorthogonal local-orbital minimum basis bandstructure scheme (FPLO) [19], within the local spin-density approximation (LSDA) [21]. For the LAPW calculation, muffin tin radii (R_{mt}) were set so that neighboring muffin tin spheres were nearly touching at each volume, and the plane wave cutoff K_{max} was determined by $R_{mt}K_{max} = 9.0$. The Brillouin zone was sampled on a uniform mesh with 185 irreducible k-points. The energy convergence criterion was set to 0.1 mRy. For both calculations we found it necessary to put the lithium 1s core electrons into the valence states. Thus, in the FPLO scheme, Li 1s, 2s, 3p, 3s, 3p and 3d states and N 2s, 2p, 3s, 3p and 3d states were used as valence states and only the lower-lying N 1s state was treated as a core state. The results of these two codes are in good agreement.

RESULTS

X-ray Diffraction

X-ray diffraction results up to 200 GPa are summarized in Figures 1 and 2. At ambient conditions, the powder sample exists as a combination of two hexagonal phases known as α-Li_3N (P6/mmm) and metastable β-Li_3N ($P6_3/mmc$). α-Li_3N fully transforms to β-Li_3N near 0.5 GPa, and a second phase transition to a cubic phase, γ-Li_3N (Fm3m), occurs near 40 GPa. The cubic phase can be understood as the rocksalt structure with the two additional Li ions occupying the tetrahedral holes in the lattice. The additional diffraction lines seen at 200 GPa are from grains of copper in the sample chamber which were used as pressure indicators.

In Figure 2, experimental data showing the change in volume as a function of pressure for β- and γ-Li_3N are fit with the 3rd order Birch-Murnaghan equation of state

$$P = \frac{3}{2}B_0(v^{-7/3} - v^{-5/3})\left[1 + \frac{3}{4}(B_0' - 4)(v^{-2/3} - 1)\right] \quad (1)$$

where $v = (V/V_0)$. Fitting parameters are summarized in Table 1, and compared with results from previous studies. Equation of state from DFT calculations is also shown as the dotted lines in Fig. 2 and the fitting parameters compared to experimental data in Table 1. The agreement between experiment and theory is quite good, indicating that the approximations made in the calcu-

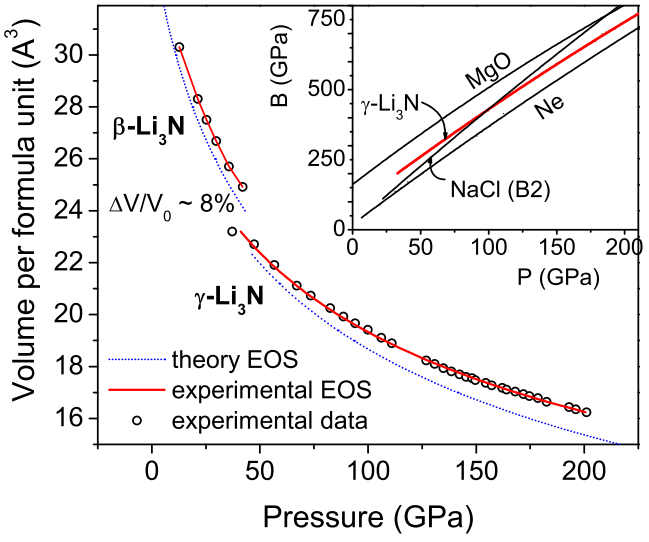

FIG. 2: (Color online) Experimental and calculated equation of state of β- and γ-Li_3N. In the inset, the high pressure bulk modulus of γ-Li_3N is compared to other common highly compressible materials. [22, 23] (NaCl, MgO and Ne Curves are interpolated up to 200 GPa).

lations are appropriate for this system. Differences between experimental and calculated equation of state in the cubic phase are likely due to the lack of a pressure medium in the highest pressure experimental study. However, the lack of broadening of the diffraction peaks between 43 and 200 GPa in the γ phase indicate very little inhomogeneous strain and, therefore, quasihydrostatic conditions.

In the inset of Figure 2 we examine the change in bulk modulus (a measure of the compressibility) as a function of pressure for cubic Li_3N and compare it with isoelectronic neon, as well as other well-known and highly compressible closed-shell ionic solids. Interestingly, in spite of the fact that the highly charged nitrogen ions may be expected to be subject to a significant coulomb repulsion at high pressure which would result in a large increase in bulk modulus, the cubic phase follows the same trend in compressibility as inert neon. It appears that the N ions are very effectively screened from one another by a full shell of 14 Li^+ ions, stabilizing the compound in the closed-shell ionic state up to surprisingly high pressure. The high compressibility and phase stability, simple diffraction pattern and low electron density in this material indicate a possible use as an internal pressure calibrant for x-ray diffraction studies of lightweight materials at high pressure. For further details concerning the structural phase transitions, see [14].

TABLE I: Volume per formula unit V_o, bulk modulus B_o, its pressure derivative $B_o{}''$, volume change at the $\beta \rightarrow \gamma$ transition and transition pressure as obtained in experimental(*) and theoretical work in present and other studies. Experimental errors are primarily a result of non-hydrostaticity in the DAC. The γ-phase predicted in reference [13] is space group $P\bar{4}3m$.

		V_0 ($\frac{\mathring{A}^3}{f.u.}$)	B_0(GPa)	$B_0{}'$	$\frac{\Delta V}{V_0}$	P(GPa)
Exp.*	β	34.4(.8)	71(19)	3.9(.9)	8(2)%	40(5)
	γ	30.8(.8)	78(13)	4.2(.2)		
Th.	β	34.44(.08)	68(3)	3.6(.1)	6.7%	40.4
	γ	31.16(.08)	73.1(.8)	3.85(.01)		
[13]*	β	35.04	74(6)	3.7(.7)		>35
[13]	β	30.88	78.2	3.77	8%	37.9
	γ	28.08	82.8	3.84		
[25]	β	33.36				28(5)
	γ	30.44				
[24]*	β	34.48				>10

*Experimental Results

X-Ray Raman Scattering

While structurally similar to the graphite-diamond and hexagonal-cubic BN transitions, the different bonding in Li_3N (ionic rather than covalent) led us to examine the electronic structure with X-ray Raman spectroscopy (XRS), with which one can probe the k-shells of low-Z materials (in our case, nitrogen). The acquired spectra (Figure 3) describe the density of electronic transitions from the nitrogen core to the lowest lying unoccupied conduction states. In the case of the covalently bonded materials, the XRS spectrum is characterized by two distinct features: a sharper peak at lower energy which has been shown to correspond to transitions to π^* molecular orbital states, and a broader peak at higher energy which describes transitions to σ^* states [26–28]. The phase transition from a layered hexagonal structure such as graphite to a more isotropic cubic structure such as diamond is accompanied by a change from sp^2 to sp^3 bonding types. An sp^2-bonded solid has a sizable proportion of π^* bonding states which are completely absent in an sp^3 bonded material. Therefore, one sees the narrower lower energy peak disappear across the hexagonal-cubic transition in the covalently bonded compounds. The data acquired for Li_3N (Figure 3) show the same characteristic leading edge peak in both hexagonal phases and not in the cubic phase.

However, the calculated spectra reveal some important differences. Within the dipole approximation, and disregarding possible excitonic effects, the nitrogen k-edge XRS should give us a reasonably good approximation of the X-ray absorption spectrum. We therefore calculated this quantity from the nitrogen p projected density of states multiplied by the dipole-allowed transition matrix elements and a transition probability (Figure 3). The

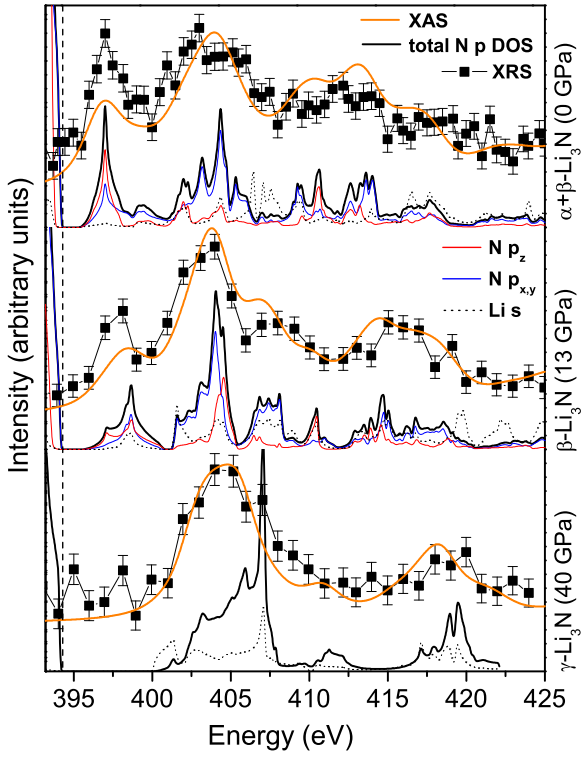

FIG. 3: (Color online) Measured nitrogen k-edge XRS spectra from the three phases of Li_3N compared with calculated Nitrogen p and Lithium s projected density of states and with the calculated x-ray absorption spectrum. The calculated curves were offset by 394.2 eV (arbitrary) in every case, for the sake of qualitative comparison with the experimental results.

important features in the experimental spectrum are reproduced reasonably accurately in the calculated X-ray absorption spectrum and in the nitrogen p projected density of states. The projected density of states is shown for the purpose of demonstrating one important point; the leading edge peak (which, in the case of graphite, represents a π^* bonding state of almost entirely C p_z character [29]) is composed of nearly equal contributions from p_z and p_x+p_y. This indicates that the nitrogen p states in hexagonal Li_3N are energetically indistinguishable; their distribution is spherically symmetric, with little directional character. This is good evidence in support of a closed-shell ionic state and raises interesting questions about the nature of this leading edge peak. Why is it present in the hexagonal phase and not in the cubic, if the p electron states are not significantly affected by changes in local coordination?

Electronic structure interpretations of ambient Li_3N from previous work claim that the electronic bands from which this density arises have Li 2s character [1]. We plot the bandstructures for the three phases (Figure 4), and, from the symmetry of the band in question (highlighted), it appears this is indeed a reasonable interpretation. In the α phase, the band has a minimum with parabolic character around the Γ point and has Γ_1^+ symmetry, as is expected for the s-band. β-Li_3N has two formula units per primitive cell, so the (symmetric) Γ_1^+ band folds back at the Brillouin zone boundary, giving rise to a second band with (antisymmetric) Γ_3^+ symmetry (notation taken from Robertson [30]). The projected density of Li s states (black dotted curve in Figure 3) compared to nitrogen p, however, show insignificant s contribution to this band, particularly in the α phase. It appears that a different interpretation altogether is needed for this low-energy conduction band.

DISCUSSION

We suggest the identity of the low energy band from another comparison with graphite and hexagonal boron nitride. These materials, in addition to the π^* and σ^* states in the absorption spectrum, possess a smaller and weaker peak, the existence of which has been long known but generally ignored because of its overlap with the much more dominant sp bands [31–33]. Its character, however, is well understood and in fact very recently it has been suggested to play a vital role in the superconductivity of the lithium intercalated graphite compounds [34]. This band is a free-electron-like interlayer (IL) state (much less well separated from the other electronic bands than in Li_3N) which is manifested as a concentration of electron states in the interstitial region between the hexagonal layers. This state tends to hybridize with the more dispersed atomic states in the system; in our case nitrogen p states.

An examination of the charge density originating from the IL band in Li_3N (Figures 5 and 6) indeed reveals, in the hexagonal phases, a concentration of electron density in the more open interstitial regions between the hexagonal planes. The charge density associated with the very large N^{3-} ions is extended far into the IL regions, such that the IL state adopts a significant amount of N p character, which is evident from the N-atom-like charge densities we see in this energy range.

The IL bands in this material differ from those seen in graphite and graphite intercalates and also h-BN in several ways. The effective band masses at the conduction band minima for α and β-Li_3N are $0.36m_o$ and $0.46m_o$, respectively, which is a significant deviation from free electron-like behavior. Also, the IL bands show a large dispersion along k_z (Γ-A), indicating that the states are not strongly confined between the hexagonal layers in this material. Between 0 and 35 GPa in the β phase, the energy of the IL band (particularly at the minimum at K) does not change (Figure 7) as greatly as that of the lithium intercalates which exhibit a marked increase

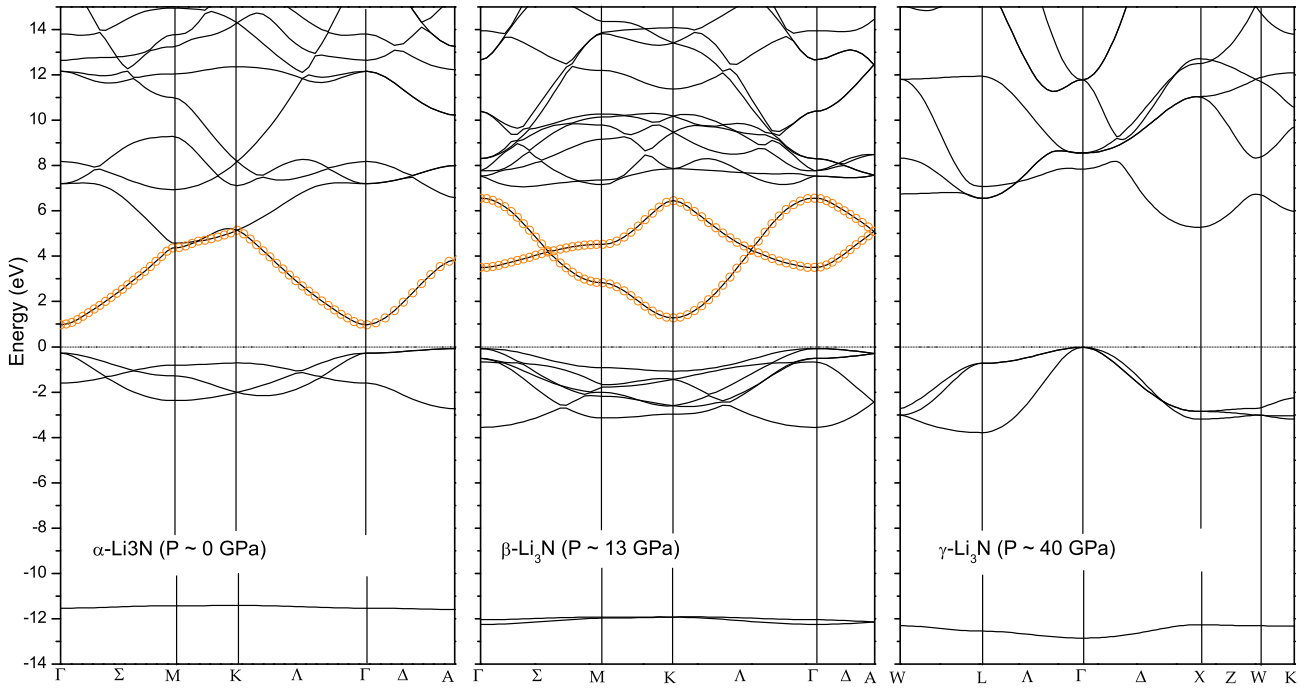

FIG. 4: (Color online) Calculated electronic band structure for the three phases of Li_3N, with the interlayer band highlighted in orange in the two hexagonal phases.

of IL band energy with decreasing c-axis lattice constant [34, 35]. The increased stability and lack of free-electron-like character in the IL bands of hexagonal Li_3N phases are likely due to the presence of Li ions between the layers, which serve to break up the interlayer space and create disconnected regions of charge.

Within the dipole approximation (limit of small momentum transfer q), the XRS spectrum replicates the x-ray absorption spectrum and transitions from the core to an IL final state would not be allowed (except in the case of a specifically oriented single-crystal sample [29]). At larger values of q, however, non dipole-allowed transitions can contribute to the spectrum. In our case, q $\sim$2.2 $Å^{-1}$; too large for the dipole approximation to be very good. However, within the dipole limit the N k-edge XRS should show only final states with N 2p character and we do see good agreement between the XRS and N p projected DOS. This suggests that transitions to the IL state are primarily only allowed to the extent that it is hybridized with the nitrogen p states, and the intensity of the leading edge peak is a measure of the degree of that hybridization. The XRS, therefore, provides an indirect measurement of the presence of an IL state, but the intensity of the leading edge peak may not represent its full extent.

The existence of the IL band could also explain the lack of sharp onset to the leading edge peak often seen in XRS due to excitonic effects. In cases where the electronic transition is 1s $\rightarrow \pi^*$ on a single atom, one has a core hole and electron in close enough proximity for an exciton to be created. If the transition is to an interlayer region, however, the core hole will be far enough away that exitonic effects will be less, and we will not see such a sharp onset [36].

In this model, the large increase in band gap across the phase transition from hexagonal β-Li_3N to cubic γ-Li_3N can be understood simply as a loss of the IL band. The cubic structure is close-packed; it does not contain empty interstitial regions large enough for electronic states with non-atomic character to exist. The implication then is that in this regime pressure is not moving the system toward a covalent or metallic system (the typical behavior as bands broaden) but instead into an even more ionic state. In the cubic phase we see more localized and sym-

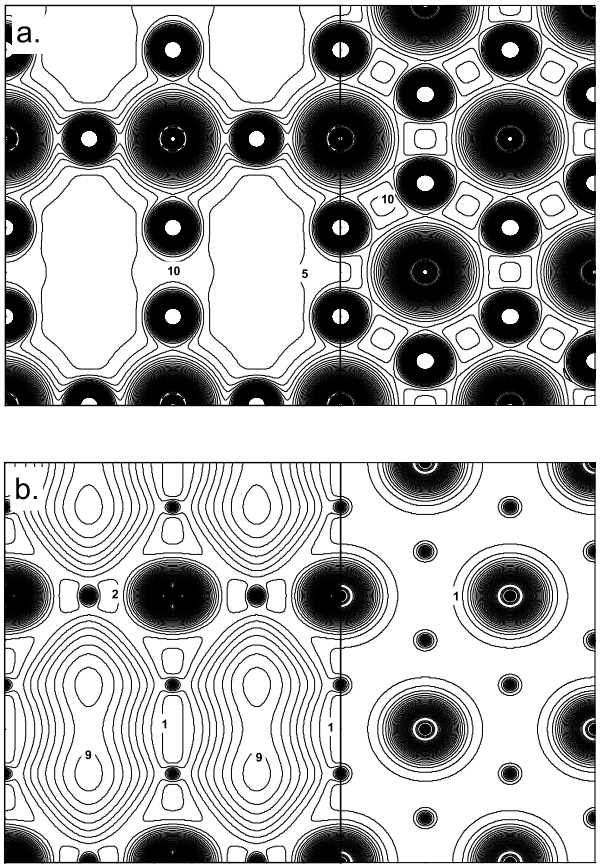

FIG. 5: Valence (a) and interlayer (b) α-Li_3N charge densities perpendicular to the basal plane (left panels) and within the basal plane (right panels). Contours are labeled in units of 0.01 e/$\AA^3$ and separated by 0.05 e/$\AA^3$ (a) and 0.01 e/$\AA^3$ (b).

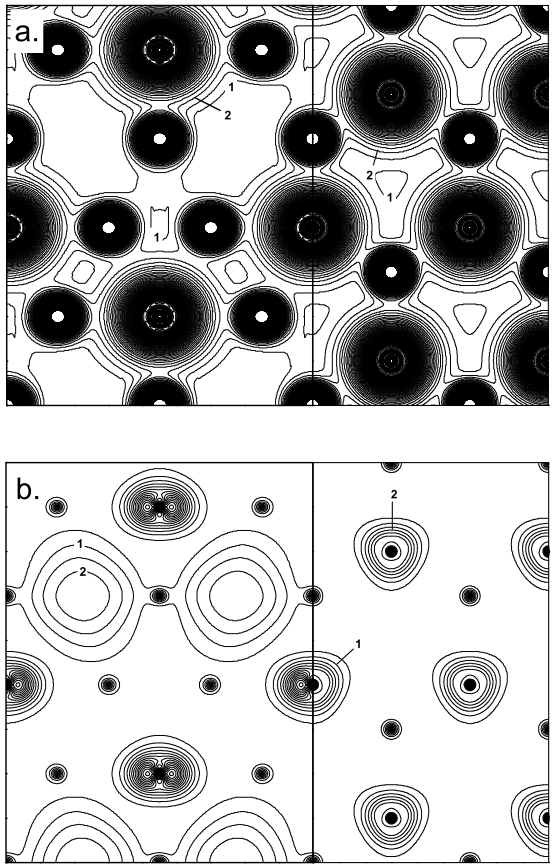

FIG. 6: Valence (a) and interlayer (b) β-Li_3N charge densities perpendicular to the basal plane (left panels) and within the basal plane (right panels). Contour lines are labeled in units of 0.1 e/$\AA^3$ and separated by 0.05 e/$\AA^3$.

metric charge distributions around the nitrogen atoms, making them even closer to the ideal N^{3-} state and explaining the insulating character and high stability of this phase.

The large bandgap increase is evident experimentally from the change in optical absorption near the phase transition (Figure 8). The calculated band gap increases from $\beta \rightarrow \gamma$ is 1.5 to 5.5 eV (the GGA tends to cause an underestimate of the gap). At 5.5 eV we may expect to see a completely transparent sample but, in fact, we see a strong yellow-orange tint (corresponding to a gap in the vicinity of 2.5 eV). However, many other factors such as absorption from a color center produced by Li vacancies (which are predicted especially in the hexagonal phases, as a driving force for superionic conductivity [37]) could cause such a coloration.

The calculated behavior of the γ-Li_3N band gap upon further increase of pressure is shown in Figure 9. As volume is reduced, the $\sim$ 5.4 eV indirect fundamental gap between Γ and X begins to increase rapidly, passing the band minimum at L near $V/V_0 = 0.4$. The Γ-L indirect

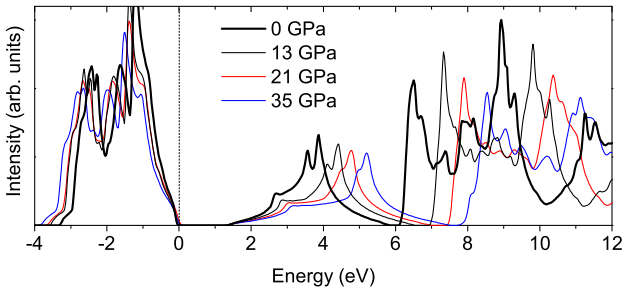

FIG. 7: (Color online) Total density of states of valence and low-lying conduction bands of β-Li_3N between 0 and 35 GPa.

gap continues to increase more slowly up to $\sim$8.2 eV at $V/V_o = 0.22$ (calculated pressure of $\sim$760 GPa), before finally beginning to collapse. Metallization via closing of the Γ-L gap finally occurs at $V/V_o = 0.08$ (calculated pressure of $\sim$8 TPa, which is a lower limit due to the known GGA misrepresentation of band gaps.) The gap closing is due to broadening of the valence and conduction bands; the band centers, however, continue to sep-

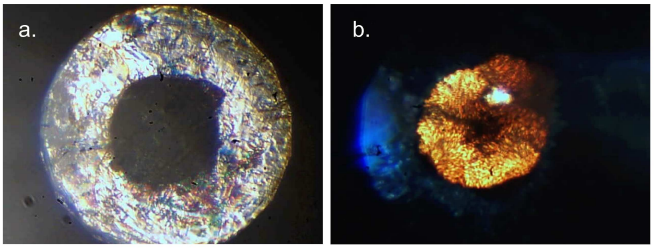

FIG. 8: (Color online) Sample image at ambient pressure (a) and at the $\beta \rightarrow \gamma$ phase transition near 40 GPa (b). The bright spot at 40 GPa is the ruby grain used for pressure calibration.

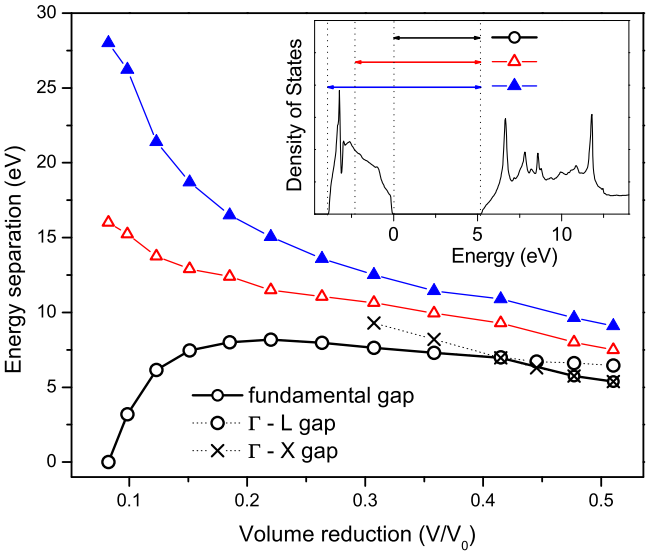

FIG. 9: (Color online) Change in valence band energies relative to bottom of the conduction band in the γ phase from the phase transition to metallization. Energy gaps explained in the density of states plot (inset): open circles give the fundamental band gap, and the energy separation between the bottom of the conduction band and the center of mass of the valence band (open triangles) and the bottom of the valence band (closed triangles) are also shown. V_0 is the volume of α-Li_3N at ambient pressure.

arate throughout the entire range of pressure. By metallization, the N 2p upper valence states have broadened by a factor of 8.

To give some perspective on how high the metallization pressure is for γ-Li_3N, some of the highest metallization pressures that have ever been predicted are for other cubic close-shelled solids Ne, MgO and NaCl at 134 TPa, 21 TPa and 0.5 TPa, respectively [41–43]. Clearly, γ-Li_3N fits well into this family. This analysis neglects the possibility of an additional structural phase transition for Li_3N at higher pressures. An fcc to orthorhombic transition is conceivable [25]; however, from the example of He [44], this may not significantly effect the metallization pressure.

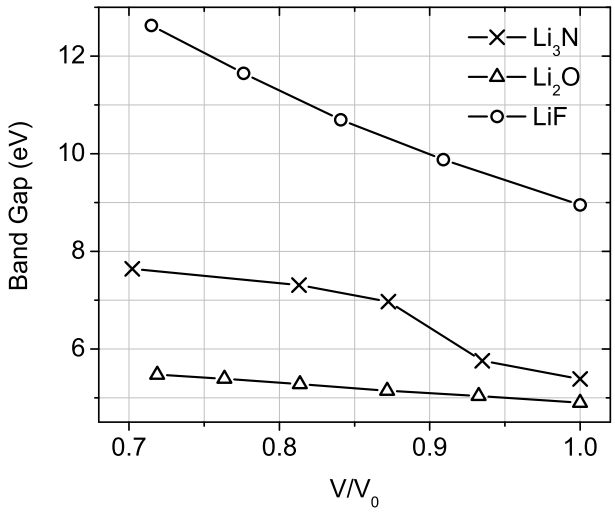

FIG. 10: Band gap increases as a function of volume reduction for related close-shelled cubic Li compounds. LiF and Li_2O are cubic at ambient pressure and V_0 refers to the ambient pressure volume. Li_3N V_0 (in this instance alone) is taken as the volume at the $\beta \rightarrow \gamma$ phase transition.

A band gap increase under pressure is observed in many other semiconducting materials; particularly the tetrahedrally coordinated zincblende and wurtzite structures such as diamond [45], group III nitrides [46, 48], and others [47]. Several effects contribute to the gap increase in these cubic semiconductors. Of primary importance is the presence of d-like states in the lower conduction or upper valence bands. The mechanism for metallization in most higher-Z ionic, insulating compounds is the strong relative decrease in energy of the conduction d bands relative to the s and p valence bands, leading to eventual transfer of electrons from d to s across the Fermi level, or hybridization between these states [49]. The reason for the record-breaking metallization pressure predicted for Ne is that the band overlap does not occur until the 3d conduction bands have fallen in energy through all the 3s and 3p conduction bands, to finally overlap the 2p valence bands at an astonishing 34-fold volume compression. This is an example of a more general trend; that bands with higher total energy (related to principle quantum number n) will increase in energy with respect to lower bands, and that bands with smaller ℓ (orbital character) increase in energy with respect to larger ℓ [49]. Indirect-gap cubic Li_3N (as well as neighboring cubic Li compounds for which we also calculated a gap increase under pressure in Figure 10, consistent with the findings of [52, 53]) have completely filled 1s shells on the lithium ions and 2p shells on the anion. The low-energy conduction bands, therefore, consist of entirely Li 2s/2p character and anion 3s/3p character (and negligibly small d character anywhere near the band gap), which can be expected to increase in energy more rapidly

than the lower-quantum number valence states, resulting in the observed band gap increase in all three of these cubic compounds.

Larger band broadening in γ-Li_3N compared to Ne due to the presence of Li ions within the fcc N^{3-} lattice results in gap closure for Li_3N at much lower compression than for Ne, long before d bands begin to overlap the valence states. This, as well as the existence of Li character in the conduction bands which makes the phenomenon more of an interspecies metallization in Li_3N, contribute to the lower metallization pressure than predicted for Ne.

The apparent correlation between cubic structure and increasing band gap can be explained in a few ways. For rocksalt compounds that do possess low-energy d bands, inversion symmetry forbids the p-d interaction at the Γ point, resulting in a repulsion between these bands at k=0. Subsequently, the direct gap increases as a function of pressure, but indirect gaps decrease as the d bands are allowed to hybridize [50, 51]. However, for the case of gap increase in the cubic phase of Li_3N (whereas the hexagonal phases show an unchanged or decreasing gap) the argument for relative trends in bands of differing orbital character appears to hold in all phases, and the fact that the fundamental gap in the hexagonal phases does not increase seems to be due simply to the more rapid band broadening. The gap between the conduction and valence states is in fact increasing in the hexagonal phases, as seen in Figure 7, but the rapid broadening of the interlayer bands as a result of the decrease in interlayer spacing (decreasing c/a ratio) causes an overall decrease in the fundamental gap.

CONCLUSION

Ionic solid Li_3N is demonstrated to possess large concentrations of unoccupied charge states in the open interlayer regions of the hexagonal phases, which result in low-energy conduction bands of the variety previously observed in layered covalently bonded compounds but not to our knowledge previously seen in ionic materials. The strong hybridization between the interlayer state and nitrogen p states allows its detection with X-ray Raman spectroscopy. The large band gap increase across the hexagonal-cubic phase transition is then interpreted as a loss of the interlayer band. Further increase of the band gap as pressure is increased is related to the rapid upward shift of the lower conduction bands relative to the valence bands, by reason of their higher angular momentum character. This band gap widening is revealed to be a general trend in the closed-shell ionic second row compounds.

ACKNOWLEDGEMENTS

We acknowledge Andy McMahon, Bruce Baer and András Libál for useful discussions during this investigation. Use of the HPCAT facility was supported by DOE-BES, DOE-NNSA (CDAC), NSF, DOD-TACOM, and the W. M. Keck Foundation. We thank HPCAT beamline scientist M. Somayazulu for technical assistance. This work has been supported by the LDRD(04ERD020) and SEGRF programs at the LLNL, University of California under DOE No. W7405-ENG-48 and by the SSAAP (DE-FG03-03NA00071) and NSF(ITR 031339) at UCD.

[1] G. Kerker, Phys. Rev. B **23**, 6312 (1981)
[2] R. Dovesi et al., Phys. Rev. B **30**, 972 (1984).
[3] E. Zintl and G. Brauer, Z. Elektrochem, **41**, 102 (1935).
[4] A. Rabenau and H. Schulz, J. Less Common Metals **50**, 155 (1976); A. Rabenau, Solid State Ionics **6**, 277 (1982).
[5] M. L. Wolf, J. Phys. C: Solid State Phys. **17**, L285 (1984).
[6] J. Sarnthein et al., Phys. Rev. B **53**, 9084 (1996).
[7] E. Bechtold-Schweickert et al., Phys. Rev. B **30**, 2891 (1984).
[8] P. Chen et al., Nature **420**, 302 (2002).
[9] T. Ichikawa et al., J. Alloys Compd. **365**, 271 (2004).
[10] Y. H. Hu et al., Ind. Eng. Chem. Res. **44**, 1510 (2005).
[11] Y. Nakamori et al., Appl. Phys. A: Mat. Sci. Process. **80**(1): 1 (2005).
[12] Y Xie et al., Science **272**, 1926 (1996).
[13] A. C. Ho et al., Phys. Rev. B **59**, 6083 (1999).
[14] A Lazicki, B. Maddox, W. J. Evans, C.-S. Yoo, A. K. McMahan, W. E. Pickett, R. T. Scalettar, M. Y. Hu and P. Chow, Phys. Rev. Lett. **95**, 165503 (2005).
[15] A. P. Hammersley, ESRF Internal Report, ESRF97HA02T, "FIT2D: An Introduction and Overview", (1997).
[16] S. Desgreniers and K. Lagarec, J. Appl. Cryst. **27**, 432 (1994).
[17] B. H. Toby, J. Appl. Cryst. **34**, 210 (2001).
[18] P. Blaha et al., *WIEN2k*, Karlheinz Schwarz, Techn. Universität Wien, Wien (2001).
[19] K. Koepernik and H. Eschrig, Phys. Rev. B **59**, 1743 (1999).
[20] J. P. Perdew, K. Burke, and M. Ernzerhof, Phys. Rev. Lett. **77**, 3865 (1996).
[21] J. P. Perdew and Y. Wang, Phys. Rev. B **45**, 13244 (1992).
[22] N. Sata et al., Phys. Rev. B **65**, 104114 (2002).
[23] R. J. Hemley et al., Phys. Rev. B **39**, 11820 (1989).
[24] H. J. Beister, S. Haag, R. Kniep, K. Strossner and K. Syassen, Angew. Chem. Int. Ed. **27**, 1101 (1988).
[25] J. C. Schön et al., J. Mater. Chem. **11**, 69 (2001).
[26] Y. Meng, H. Mao, P. J. Eng, T. P. Trainor, M. Newville, M. Y. Hu, C. Kao, J. Shu, D. Hausermann and R. J. Hemley, Nat. Mater. **3**, 111 (2004).
[27] S. K. Lee, P. J. Eng, H. Mao, Y. Meng, M. Newville, M. Y. Hu and J. Shu, Nat. Mater. **4**, 851 (2005).
[28] U. Bergmann, O. C. Mullins and S. P. Cramer, Anal.

Chem. **72**, 2609 (2000).
[29] P. E. Batson, Phys. Rev. B **48**, 2608 (1993).
[30] J. Robertson, Phys. Rev. B **29**, 2131 (1984).
[31] A. Catellani, M. Posternak, A. Baldereschi, H. J. F. Jansen and A. J. Freeman, Phys. Rev. B **32**, 6997 (1985).
[32] B. Reihl, J. K. Gimzewski, J. M. Nicholls and E. Tosatti, Phys. Rev. B **33**, 5770 (1986).
[33] Th. Fauster, F. J. Himpsel, J. E. Fischer and E. W. Plummer, Phys. Rev. Lett. **51**, 430 (1983).
[34] G. Csányi, P. B. Littlewood, A. H. Nevidomskyy, C. J. Pickard and B. D. Simons, Nature Physics **1**, 42 (2005).
[35] X. Blase, A. Rubio, S. G. Louie and M. L. Cohen, Phys. Rev. B **51**, 6868 (1995).
[36] A. Koma, K. Miki, H. Suematsu, T. Ohno and H. Kamimura, Phys. Rev. B **34**, 2434 (1986).
[37] H. Schulz and K. H. Thiemann, Acta Cryst. **A35**, 309 (1979).
[38] R. Buczko, G. Duscher, S. J. Pennycook and S. T. Pantelides, Phys. Rev. Lett. **85**, 2168 (2000).
[39] A. Soininen, Academic Dissertation, University of Helsinki (2001).
[40] E. L. Shirley, Phys. Rev. Lett. **80**, 794 (1998); Eric L. Shirley, J. A. Soininen, G. P. Zhang, J. A. Carlisle, T. A. Callcott, D. L. Ederer, L. J. Terminello and R. C. C. Perera, J. of Electron Spectrosc. Relat. Phenom. **114-116**, 939 (2001).
[41] J. C. Boettger, Phys. Rev. B **33**, 6788 (1986).
[42] A. R. Oganov, M. J. Gillan, G. D. Price, J. Chem. Phys. **118**, 10174 (2003).
[43] J. L. Feldman, B. M. Klein, M. J. Mehl and H. Krakauer, Phys. Rev. B **42**, 2752 (1990).
[44] D. A. Young, A. K. McMahan and M. Ross, Phys. Rev. B **24**, 5119 (1981).
[45] S. Fahy, K. J. Chang, S. G. Louie and M. L. Cohen, Phys. Rev. B **35**, 5856 (1987).
[46] R.M. Wentzcovitch, K. J. Chang and M. L. Cohen, Phys. Rev. B **34**, 1071 (1986).
[47] D. L. Camphausen, G. A. N. Connell and W. Paul, Phys. Rev. Lett. **26**, 184 (1971).
[48] K. Kim, W. R. L. Lambrecht and B. Segall, Phys. Rev. B **53**, 16310 (1996).
[49] A. K. McMahan, Physica B+C, **139-140**, 31 (1986); A. K. McMahan and R. C. Albers, Phys. Rev. Lett. **49**, 1198 (1982).
[50] S. Ves, U. Schwarz, N. E. Christensen, K. Syassen and M. Cardona, Phys. Rev. B **42**, 9113 (1990).
[51] P. E. Van Camp, V. E. Van Doren and J. T. Devreese, Phys. Rev. B **38**, 9906 (1988).
[52] J. Clérouin, Y. Laudernet, V. Recoules and S. Mazevet, Phys. Rev. B **72**, 155122 (2005).
[53] A. Zunger and A. J. Freeman, Phys. Rev. B **16**, 2901 (1977).